Research Article | Vol. 26, No. 11 | 28 May 2018 | OPTICS EXPRESS 14800
Optics EXPRESS

Ultra-broadband multimode 3dB optical power splitter using an adiabatic coupler and a Y-branch

LIANGSHUN HAN,[1,*] BILL P.-P. KUO,[1] NIKOLA ALIC,[2] AND STOJAN RADIC[1]

[1]*Department of Electrical and Computer Engineering, University of California, San Diego, La Jolla, CA 92093 USA*
[2]*California Institute for Telecommunications and Information Technologies, University of California San Diego, La Jolla, CA 92093 USA*
**lih076@ucsd.edu*

Abstract: As an essential component of mode division multiplexing (MDM) system, a multimode 3dB power splitter with low loss, high power balance, and low mode crosstalk is highly desired. In this paper, we propose an ultra-broadband on-chip multimode 3dB optical power splitter using an adiabatic coupler and an S-bend based Y-branch. As an example, a splitter for the four-lowest modes of a rib waveguide on silicon on insulator (SOI) platform is designed. Simulation results show that the device exhibits < 0.12dB insertion losses, within ± 0.38dB power imbalances, and < −18.5dB mode crosstalks for the four-lowest modes within a large operating wavelength range of 165 nm (from 1400 nm to 1565 nm). The fabrication tolerance of gap size at the output end of the adiabatic coupler is also analyzed.

OCIS codes: (130.3120) Integrated optics devices; (060.4230) Multiplexing; (230.1360) Beam splitters; (130.2790) Guided waves.

References and links

1. A. Shacham, K. Bergman, and L. P. Carloni, "Photonic Networks-on-Chip for Future Generations of Chip Multiprocessors," IEEE Trans. Comput. **57**(9), 1246–1260 (2008).
2. D. Miller, "Device Requirements for Optical Interconnects to Silicon Chips," Proc. IEEE **97**(7), 1166–1185 (2009).
3. K. Ohashi, K. Nishi, T. Shimizu, M. Nakada, J. Fujikata, J. Ushida, S. Torii, K. Nose, M. Mizuno, H. Yukawa, M. Kinoshita, N. Suzuki, A. Gomyo, T. Ishi, D. Okamoto, K. Furue, T. Ueno, T. Tsuchizawa, T. Watanabe, K. Yamada, S. Itabashi, and J. Akedo, "On-Chip Optical Interconnect," Proc. IEEE **97**(7), 1186–1198 (2009).
4. P. Dong, "Silicon Photonic Integrated Circuits for Wavelength-Division Multiplexing Applications," IEEE J. Sel. Top. Quantum Electron. **22**(6), 370–378 (2016).
5. A. Liu, L. Ling, Y. Chetrit, J. Basak, H. Nguyen, D. Rubin, and M. Paniccia, "Wavelength Division Multiplexing Based Photonic Integrated Circuits on Silicon-on-Insulator Platform," IEEE J. Sel. Top. Quantum Electron. **16**(1), 23–32 (2010).
6. L.-W. Luo, N. Ophir, C. P. Chen, L. H. Gabrielli, C. B. Poitras, K. Bergmen, and M. Lipson, "WDM-compatible mode-division multiplexing on a silicon chip," Nat. Commun. **5**(1), 3069 (2014).
7. L. Han, S. Liang, J. Xu, L. Qiao, H. Zhu, and W. Wang, "Simultaneous Wavelength- and Mode-Division (De)multiplexing for High-Capacity On-Chip Data Transmission Link," IEEE Photonics J. **8**(2), 1–10 (2016).
8. J. Wang, P. Chen, S. Chen, Y. Shi, and D. Dai, "Improved 8-channel silicon mode demultiplexer with grating polarizers," Opt. Express **22**(11), 12799–12807 (2014).
9. S. Wang, H. Wu, H. K. Tsang, and D. Dai, "Monolithically integrated reconfigurable add-drop multiplexer for mode-division-multiplexing systems," Opt. Lett. **41**(22), 5298–5301 (2016).
10. L. Han, S. Liang, H. Zhu, L. Qiao, J. Xu, and W. Wang, "Two-mode de/multiplexer based on multimode interference couplers with a tilted joint as phase shifter," Opt. Lett. **40**(4), 518–521 (2015).
11. Y. Ding, J. Xu, F. Da Ros, B. Huang, H. Ou, and C. Peucheret, "On-chip two-mode division multiplexing using tapered directional coupler-based mode multiplexer and demultiplexer," Opt. Express **21**(8), 10376–10382 (2013).
12. B. Stern, X. Zhu, C. P. Chen, L. D. Tzuang, J. Cardenas, K. Bergman, and M. Lipson, "On-chip mode-division multiplexing switch," Optica **2**(6), 530 (2015).
13. C. Sun, Y. Yu, G. Chen, and X. Zhang, "On-chip switch for reconfigurable mode-multiplexing optical network," Opt. Express **24**(19), 21722–21728 (2016).
14. L. H. Gabrielli, D. Liu, S. G. Johnson, and M. Lipson, "On-chip transformation optics for multimode waveguide bends," Nat. Commun. **3**(1), 1217 (2012).

#328306 https://doi.org/10.1364/OE.26.014800
Journal © 2018 Received 17 Apr 2018; revised 22 May 2018; accepted 22 May 2018; published 25 May 2018

Optics EXPRESS

15. Y. Luo, Y. Yu, M. Ye, C. Sun, and X. Zhang, "Integrated dual-mode 3 dB power coupler based on tapered directional coupler," Sci. Rep. **6**(1), 23516 (2016).
16. H. Xu and Y. Shi, "Ultra-broadband dual-mode 3 dB power splitter based on a Y-junction assisted with mode converters," Opt. Lett. **41**(21), 5047–5050 (2016).
17. J. Xing, K. Xiong, H. Xu, Z. Li, X. Xiao, J. Yu, and Y. Yu, "Silicon-on-insulator-based adiabatic splitter with simultaneous tapering of velocity and coupling," Opt. Lett. **38**(13), 2221–2223 (2013).
18. A. Yariv, "Coupled-mode theory for guided-wave optics," IEEE J. Quantum Electron. **9**(9), 919–933 (1973).
19. X. Sun, H.-C. Liu, and A. Yariv, "Adiabaticity criterion and the shortest adiabatic mode transformer in a coupled-waveguide system," Opt. Lett. **34**(3), 280–282 (2009).
20. D. Dai, Y. Tang, and J. E. Bowers, "Mode conversion in tapered submicron silicon ridge optical waveguides," Opt. Express **20**(12), 13425–13439 (2012).

1. Introduction

To satisfy the ever-increasing traffic demands on high-speed data transmission for data-intensive applications, on-chip optical interconnection has obtained extensive attentions due to its high-bandwidth, low power consumption, and compact size [1–3]. A wide range of techniques have been deeply studied to improve the capacity of on-chip optical interconnection, such as wavelength division multiplexing (WDM), polarization division multiplexing, and advanced modulation formats. Among them, WDM is one straightforward way to enable high capacity by transmitting multiple wavelengths on the same optical path [4,5]. However, the requirement of multiple lasers with different wavelengths could be expensive for an on-chip optical interconnection link. Recently, a new multiplexing technique termed as mode division multiplexing (MDM) for on-chip optical interconnection has been proposed by simultaneously using different guided modes as independent signal carriers to transfer signals, which provides a new dimension to expand the capacity in a single wavelength channel [6–8]. What's more, MDM technique could also be used to build flexible optical networks such as reconfigurable optical add/drop multiplexing (ROADM) [9]. Consequently, combined with other techniques, MDM technique could offer a higher capacity and more flexible on-chip optical interconnection scheme.

In order to realize a MDM system, many on-chip devices including mode (de)multiplexer [6,10,11], switches [12,13], and bent waveguides [14] have been studied to be fully compatible with high-order modes. However, still to now, only a few studies have been performed to achieve multimode power splitters for on-chip MDM systems. In [15], a 3dB power splitter for TM_0 and TM_1 modes based on a well optimized tapered directional coupler has been fabricated on silicon on insulator (SOI) wafer. The basic design concept is to find the common multiple of 3dB coupling lengths for the two modes, which also indicates that this design is hard to be extended to process more modes or higher-order modes. Another device reported in [16] employs cascaded structure to separately split different modes by a Y-branch. Before splitting process, a N^{th}-order mode needs to be converted to a $2N^{th}$-order mode first, imposing complexity on device structure as mode number increases.

In this paper, we propose an ultra-broadband multimode 3dB power splitter consisting of only an adiabatic coupler and a symmetric Y-branch to further simplify device structure and expand the mode capacity. A similar structure was studied as a fundamental mode (TE_0) 3dB power splitter in [17], showing large operating bandwidth and fabrication tolerance in adiabatic region length. Here we will focus on multimode power splitting process. In principle, the mode capacity of this design is mainly determined from the number of modes supported by input waveguide and required crosstalk level between different modes. To validate this design, a splitter for processing four-lowest guided modes (TE_0, TE_1, TE_2, and TM_0) of a multimode SOI waveguide is considered in this paper as an example. Numerical simulation demonstrates that this design possesses < 0.12dB insertion losses with lower than −18.5dB mode crosstalks within a record-large 165nm wavelength range. Besides, we further analyze the fabrication tolerance of gap size at the output end of the adiabatic coupler, showing a robust performance under a large fabrication deviation. To the best of our

Optics EXPRESS

knowledge, this is the first study of multimode (up to four modes) 3dB power splitter based on adiabatic coupler and Y-branch.

2. Device design

2.1 Structure and principle

Figure 1(a) schematically shows a multimode 3dB power splitter consisting of two separate SOI waveguides placed close to each other in the same plane. Here, we divide this power splitter into two functional parts: an adiabatic coupler (AC) and a symmetric Y-branch. In the AC part, the two waveguides are firstly designed with different widths (W_{WG1} and W_{WG2}) and large gap (G_{in}) to avoid unwanted interference. Then, they are linearly tapered to a same width W_{out} and the gap decreases from G_{in} to G_{AC} gradually, forming an adiabatic coupled-waveguide system. In the Y-branch, the two waveguides are finally pulled away to a large separation (G_{out}) to realize mode decoupling, and the widths keep constant to make the power evenly split into the two waveguides.

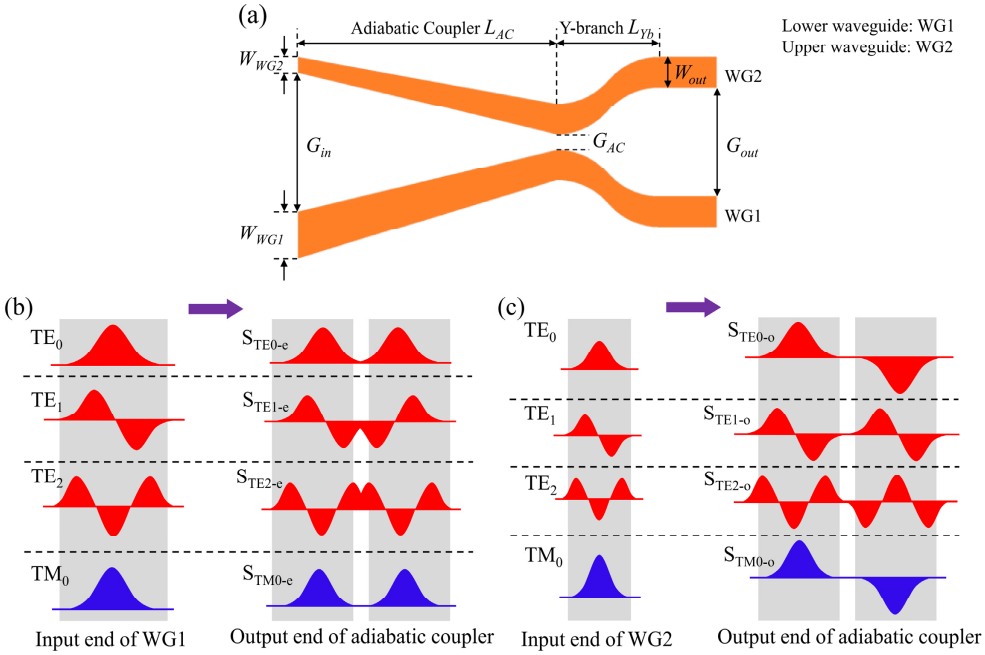

Fig. 1. (a) Top view schematic of the proposed multimode 3dB power splitter with section indications; Relationships between normal modes and excited supermodes for using (b) WG1 and (c) WG2 as the input waveguide.

By the adiabatically tapering process, one normal mode launched into WG1 (WG2) could be fully converted into the corresponding supermode at the AC's output end where phase matching happens and thus the optical power evenly distributes in the two waveguides as shown in Figs. 1(b) and 1(c). From these two figures, one can also find the relationships between the normal modes and the excited supermodes. For simplicity, we only consider four guided normal modes: TE_0, TE_1, TE_2, and TM_0 in this paper. It can be observed that the modes TE_0, TE_1, TE_2, and TM_0 in WG1 (wide waveguide) correspond to the even supermodes $S_{TE0\text{-}e}$, $S_{TE1\text{-}e}$, $S_{TE2\text{-}e}$, and $S_{TM0\text{-}e}$, respectively. In contrast, the modes TE_0, TE_1, TE_2, and TM_0 in WG2 (narrow waveguide) correspond to the odd supermodes $S_{TE0\text{-}o}$, $S_{TE1\text{-}o}$, $S_{TE2\text{-}o}$, and $S_{TM0\text{-}o}$, respectively. Note that an even supermode consists of two in-phase modes respectively confined in the two waveguides. The mode profiles in both waveguides are similar to that of the input normal mode. Unlike even supermodes, an odd supermode

Optics EXPRESS

contains two anti-phase parts. Obviously, the input normal mode could be divided into two parts without changing mode profile when the excited supermodes are launched into a symmetric Y-branch. In this way, one can realize a 3dB power splitter to simultaneously process multiple modes. It is worthwhile to note that this design could be used to process higher order normal modes TE_n and TM_n by appropriately modified waveguide cross-section dimension and length of the AC.

In this study, an SOI wafer with a 300nm-thick silicon core layer is considered as fabrication platform. Rib waveguide structure with 150nm slab height will be adopted for the device. The corresponding refractive indices of core (silicon, Si) and top/bottom cladding (silica, SiO_2) are 3.476 and 1.444 at a free space wavelength of 1550 nm, respectively. In the following, we use three-dimensional eigenmode expansion (EME) method (Lumerical Solutions, Inc) to validate and optimize the device.

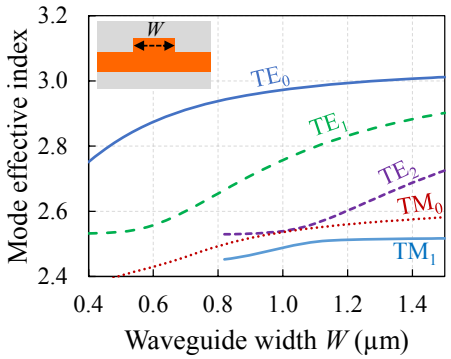

Fig. 2. Calculated mode effective indices of the four-lowest guided modes in a rib SOI waveguide with different width.

2.2 Optimization for adiabatic coupler

For a multimode photonic device, a low crosstalk between modes is highly desired. In the AC part, the mode crosstalk mainly comes from normal modes coupling between WG1 and WG2. For example, *Mode i* launched into WG1 is partially coupled into the *Mode j* in WG2 and, then, this *Mode j* will be divided into two *Mode j* at output end of Y-branch, causing *Mode i* -to- *Mode j* crosstalk ($i \neq j$). A simple approach to solve this problem is to optimize the waveguide widths to obtain significant difference between effective indices of modes in WG1 and that of modes in WG2 at the input end of the AC. Figure 2 shows the calculated mode effective indices of the four-lowest guided modes in a rib SOI waveguide with different waveguide width. One can see that the effective index of TM_0 mode is very close to that of TE_2 mode when waveguide width W approaches to 1.0 μm (determined as mode hybridization region [20] for TE_2 and TM_1 modes). In this hybridization region, the hybridized mode simultaneously contains TE_2 mode and TM_2 mode components. To minimize coupling between modes of the two waveguides, we comprehensively choose W_{WG1} and W_{WG2} as 1.4 μm and 1.0 μm, respectively. Thereby, the width of Y-branch's waveguides is W_{out} = 1.2 μm. The minimum index difference comes from TM_0 mode of WG1 and hybridized TE_2 mode of WG2.

In order to work in the adiabatic regime, the effective indices of the even (odd) supermodes should be changed slowly and smoothly enough to avoid exciting the odd (even) supermodes [18]. Simultaneously exciting even and odd supermodes could break adiabatic condition and cause deviation of power splitting ratio. The calculated effective index evolutions of the eight guided modes along the propagation direction are shown in Figs. 3(a)-3(d). The corresponding mode profiles at both in/output ends of the AC are also inset in this

Optics EXPRESS

figure. It can be seen that TE_0, TE_1, TE_2, and TM_0 in WG1 adiabatically evolve into $S_{TE0\text{-}e}$, $S_{TE1\text{-}e}$, $S_{TE2\text{-}e}$, and $S_{TM0\text{-}e}$, respectively. In contrast, $S_{TE0\text{-}o}$, $S_{TE1\text{-}o}$, and $S_{TM0\text{-}o}$ could only be adiabatically excited by TE_0, TE_1, and TM_0 in WG2, respectively, due to the closely matched effective index. Thus, it is possible to obtain adiabatically coupling between normal modes and supermodes by a long enough coupling length. Notice that Fig. 3(c) does not show the mode profile of TE_2 mode in WG2 at the input end of the AC since the corresponding mode is leaky and would be lossy in practical applications.

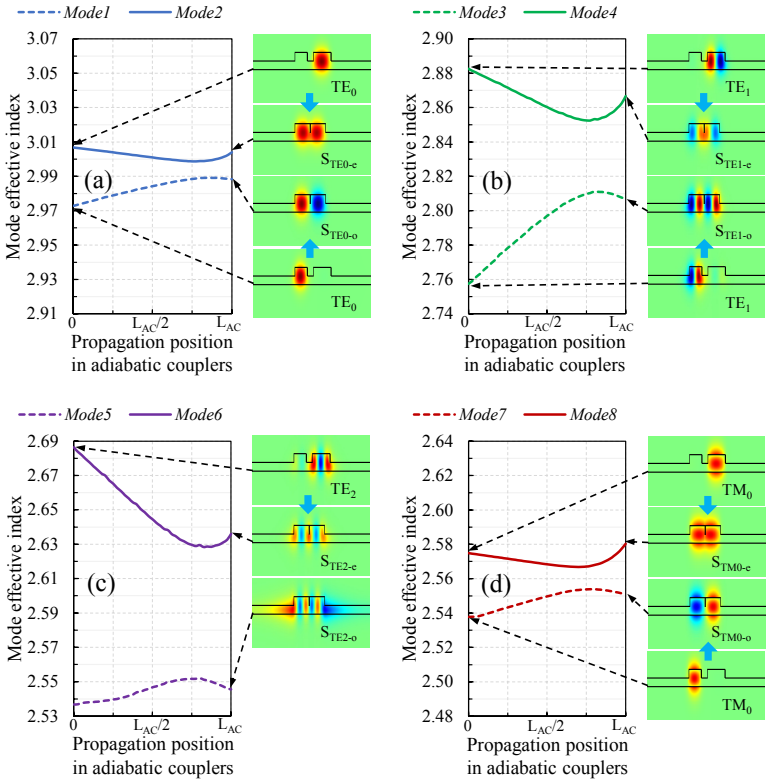

Fig. 3. Calculated the effective index evolutions of the eight guided modes along the propagation direction. (a) TE_0 mode, (b) TE_1 mode, (c) TE_2 mode, and (d) TM_0 mode are used as input for WG1 and WG2, respectively. Inset: mode profiles at both input and output end of the AC. All simulations are run at a wavelength of 1550 nm.

Theoretically, G_{in} should be large enough to realize adiabatic input and G_{AC} should be close to 0 nm to reduce coupler length resulting from enhancement of coupling strength [19]. The mode coupling at the input end of the AC is characterized through the mode filed overlaps with the adjacent waveguide. Here, we set G_{in} as 500 nm to make a trade-off between coupler length and adiabatically coupling level. In consideration of fabrication limitation, G_{AC} = 50 nm is chosen to study the relationship between adiabatically coupling length and other parameters. We simulate light propagation in the AC with different coupler lengths. The mode conversion efficiencies for the TE_0, TE_1, TE_2, and TM_0 modes respectively launched into the wide waveguide WG1 as a function of the coupler length are calculated and shown in Fig. 4(a). It can be easily seen that normal modes to even supermodes (NTS_e) conversion efficiencies increase monotonously along the coupler length. On the contrary, normal modes to odd supermodes (NTS_o) conversion efficiencies decrease monotonously with increase of coupler length. Besides, one normal mode would excite even and odd supermodes simultaneously for a short coupler length. As the coupler length increases, the

Optics EXPRESS

NTS_e conversion efficiencies become saturated and the adiabatic coupling thereby happens with negligible power coupled to excited odd supermodes. From Fig. 4(a), one can also see that the coupler length where ~100% NTS_e conversion ecoefficiency happens becomes longer when operating at a low order input mode, which is caused by weak mode coupling strength. To attain a 3dB power splitter for simultaneously processing multiple modes, the length of the AC is determined from adiabatically coupling length of the lowest normal mode (TE_0) of input port. The same results can also be obtained for a case of narrow waveguide WG2 as an input port. Therefore, we will focus on optimizing adiabatically coupling length for TE_0 mode launched into WG1.

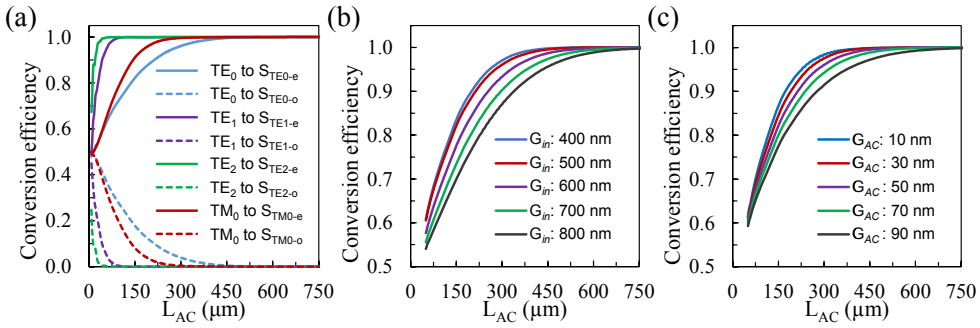

Fig. 4. (a) Calculated mode conversion efficiencies for the TE_0, TE_1, TE_2, and TM_0 modes respectively launched into the wide waveguide WG1 as a function of the length of adiabatic coupler (L_{AC}). Here, the G_{in} and G_{AC} are 50 nm and 500 nm, respectively. (b) The mode conversion efficiencies for the TE_0-to-S_{TE0-e} as a function of the AC's coupling length under different G_{in} and fixed G_{AC} = 50 nm. (c) The mode conversion efficiencies for the TE_0-to-S_{TE0-e} as a function of the AC's coupling length under different G_{AC} and fixed G_{in} = 500 nm. All simulations are run at a wavelength of 1550 nm.

Figures 4(b) and 4(c) further discuss TE_0-to-S_{TE0-e} conversion efficiencies as a function of coupler length for different G_{in} and G_{AC}, respectively. Clearly, a longer coupler length is required for a larger G_{in} or G_{AC}. To reduce fabrication sensitivity and improve operating bandwidth, the length of the AC is set as 750 μm. Figures 5(a)-5(d) show the calculated mode propagations in the AC for different mode inputs.

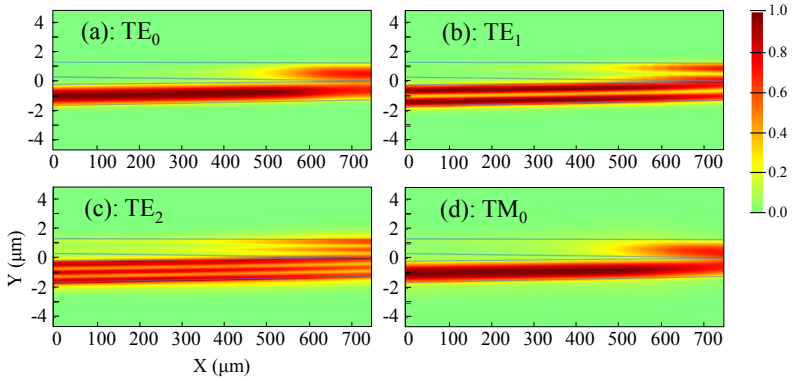

Fig. 5. Mode propagations in the AC for different modes launched into WG1 at a wavelength of 1550 nm.

2.3 Optimization for Y-branch

The symmetric Y-branch is designed with two S-bend waveguides with same width W_{out} and connects the AC and output waveguides. Here, the Y-branch serves as a splitter to divide the

Optics EXPRESS

supermode into two symmetric parts along central line (X direction). To decouple these two parts into two independent normal modes, the gap of the output end of Y-branch (G_{out}) is set as large as 2.4 μm. In Fig. 6, the relationship between length of Y-branch (L_{Yb}) and mode conversion efficiency is plotted, as calculated by mode expansion method. Due to using WG1 as input of the splitter, we only consider the cases of even supermodes as input modes for the Y-branch. The ripples in Figs. 6(a) and 6(b) shown in the curves suggest mode interference happens. Note that this kind of mode interference as one of the major sources for mode crosstalk is caused by excitation of undesired modes and could be diminished when the radius of S-bend is large enough. From Fig. 6(c), one can observe relative high $S_{TE2\text{-}e}$-to-TM_0 conversion efficiency because the $S_{TE2\text{-}e}$ dominant input mode contains a fraction of $S_{TM1\text{-}e}$ mode component when waveguide width is close to TE_2 and TM_1 mode hybridization region [20] (around W = 1.0 μm) as shown in Fig. 2. The $S_{TM1\text{-}e}$ mode component is partially converted to $S_{TM0\text{-}e}$ mode in the Y-branch, causing high $S_{TE2\text{-}e}$-to-TM_0 conversion efficiency. Nevertheless, a good power imbalance performance between two output ports is still well maintained for all four input supermodes. To obtain low-level mode crosstalk from the Y-branch, we comprehensively choose L_{Yb} to be 50 μm with an output gap size G_{out} of 2.4 μm and an over 523μm bend radius. Figure 7 shows mode propagations in the designed Y-branch for injecting $S_{TE0\text{-}e}$, $S_{TE1\text{-}e}$, $S_{TE2\text{-}e}$, and $S_{TM0\text{-}e}$ modes, respectively. Obviously, $S_{TE0\text{-}e}$, $S_{TE1\text{-}e}$, $S_{TE2\text{-}e}$, and $S_{TM0\text{-}e}$ modes are divided into two beams of TE_0, TE_1, TE_2, and TM_0 modes, respectively. Thus, this Y-branch could realize supermode splitting function. Now we obtain all parameters of the multimode 3dB power splitter presented here, as summarized in Table 1.

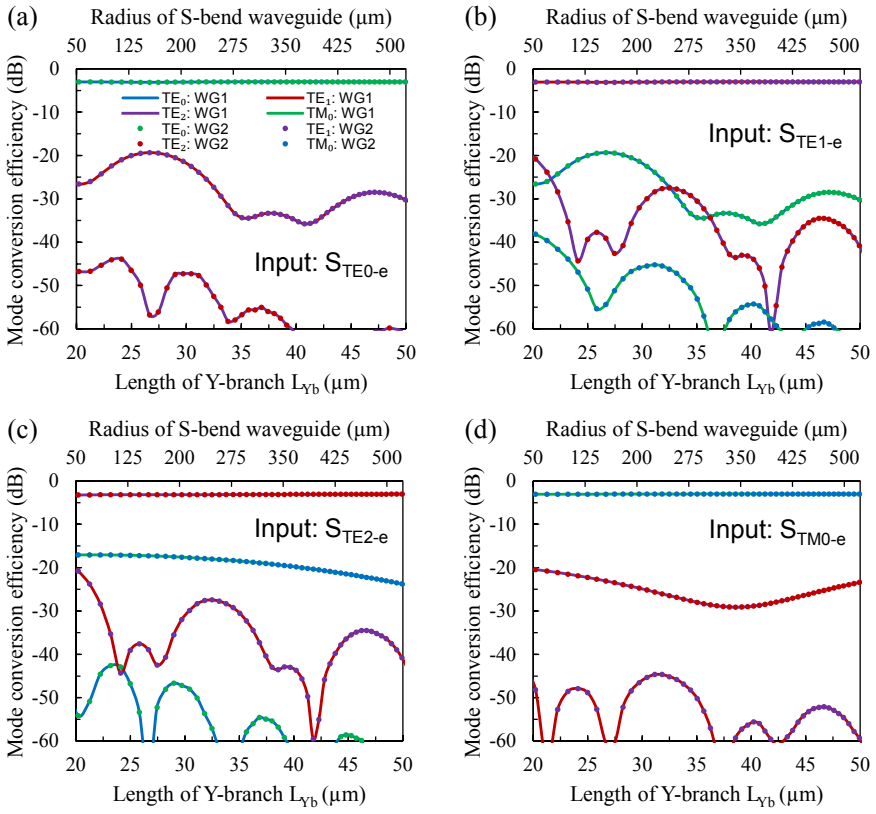

Fig. 6. Relationships between length of Y-branch (L_{Yb}) and mode conversation efficiency for different input modes in terms of (a) $S_{TE0\text{-}e}$ mode, (b) $S_{TE1\text{-}e}$ mode, (c) $S_{TE2\text{-}e}$ mode, and (d) $S_{TM0\text{-}e}$ mode. Here G_{AC} and G_{out} are 50 nm and 2.4 μm, respectively. The points with value smaller than −60 dB are not shown here. All simulations are run at a wavelength of 1550 nm.

Optics EXPRESS

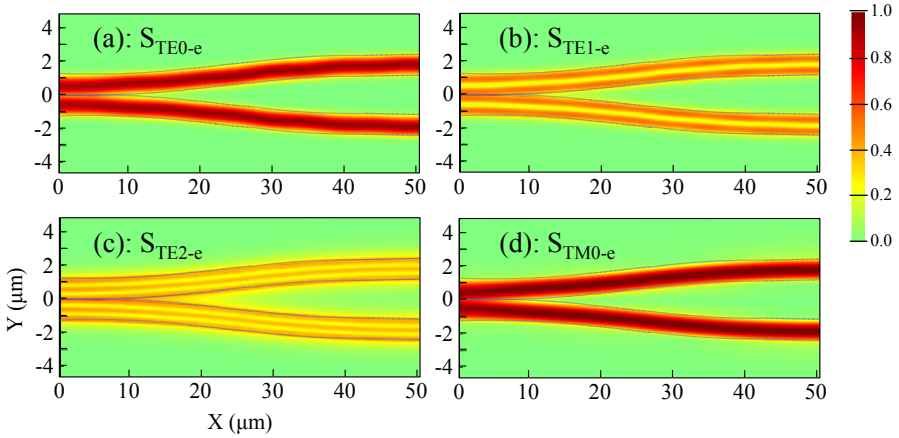

Fig. 7. Mode propagations in the Y-branch for injecting different supermodes at a wavelength of 1550 nm.

Table 1. Optimized parameters of the proposed multimode 3dB power splitter

W_{WG1} (μm)	W_{WG2} (μm)	W_{out} (μm)	G_{in} (μm)	G_{AC} (μm)	G_{out} (μm)	L_{AC} (μm)	L_{Yb} (μm)
1.4	1.0	1.2	0.5	0.05	2.4	750.0	50.0

3. Device performance and fabrication tolerance analysis

We seamlessly connect the AC and Y-branch as designed in Section 2 to further investigate the performance of a whole device. Figures 8(a)-8(d) show our obtained mode propagations at a wavelength of 1550 nm when injecting different modes into WG1. Clearly all four input modes could be well split into two output ports with unchanged mode profile, which confirms the previous simulation results for each section are reliable. Figures 9(a)-9(d) show the wavelength dependence of the insertion loss (*IL*), power imbalance (*PIMB*), and mode crosstalk (*CT*) for different input modes. These three performance parameters are defined as:

$$IL = -10\log\frac{P_{out1} + P_{out2}}{P_{in}}$$

$$PIMB = 10\log\frac{P_{out1}}{P_{out2}}$$

$$CT_i = 10\log\frac{\sum_{1,\, j\neq i}^{4} P_{out-Mode\ j}}{P_{out-Mode\ i}}$$

where P_{out1} and P_{out2} are powers collected at output ends of WG1 and WG2 in desired mode, P_{in} is the power of the desired mode launched in WG1, $P_{out-Mode\ j}$ is the total power of $Mode\ j$ converted to $Mode i$, and $P_{out-Mode\ i}$ is the output power of $Mode i$ when $Mode i$ is the input mode. The crosstalk CT_i is the summation of crosstalks from different modes. Here, the power results of different modes are extracted by using EME method. From the simulation results, ultra-low insertion losses that are less than 0.06 dB could be obtained for the four input modes at the wavelength of 1550 nm as shown in Fig. 9(a). From Fig. 9(b), one can see that this device also exhibits good power imbalances within ± 0.38 dB over the whole simulated wavelength range. Furthermore, mode crosstalks < −18.5 dB are obtained for the four modes over the wavelength band from 1400 nm to 1565 nm. Notably, the mode crosstalk for TE_2 mode degrades dramatically as operating wavelength increases, which is mainly

Optics EXPRESS

caused by the power from TM_0 mode coupled into TE_2 mode. Hence, it can be expected that mode crosstalk performances will be further improved by employing wider input waveguides to keep away from mode hybridization regions. It is also worth to underline that the operating bandwidth could be further widen up to longer wavelength side when the device only handles the three-lowest TE modes. These simulated results indicate that the proposed multimode 3dB power splitter possesses a good insensitivity to working wavelength as other adiabatically coupling based devices do.

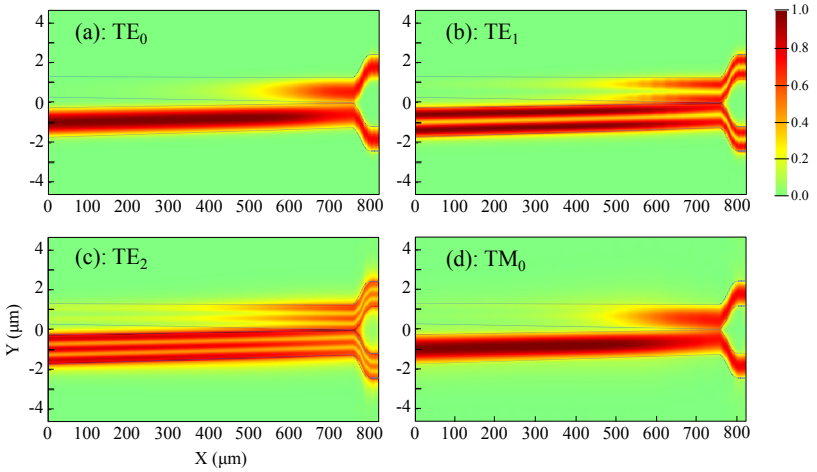

Fig. 8. Mode propagations in the whole device for different modes launched into WG1 at a wavelength of 1550 nm: (a) TE_0 mode, (b) TE_1 mode, (c) TE_2 mode, and (d) TM_0 mode.

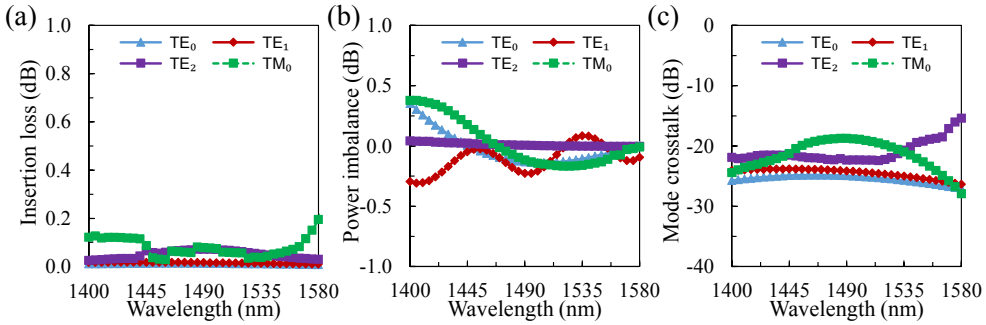

Fig. 9. Wavelength dependence of the proposed device performance in terms of (a) insertion loss, (b) power imbalance, and (c) mode crosstalk.

Next, the fabrication tolerance of the designed splitter is investigated. We simulate the performance variations due to fabrication errors from gap size G_{AC} which is the smallest geometrical parameter. In our simulations, the operating wavelength is fixed at 1550 nm and only G_{AC} is swept while other parameters are kept at the nominal values shown in Table 1. Figure 10 plots the simulation results showing a very stable performance even for a large deviation of 40 nm, which benefits from adopting a long enough L_{AC}. Therefore, our proposed device could be reliably fabricated by using electron-beam lithography process and single step inductively coupled plasma etching process. To relief the requirement from lithography resolution, it is also possible to employ a large G_{AC} to enable the same splitting function at the expense of a large device footprint, particularly in adiabatic coupler length.

Optics EXPRESS

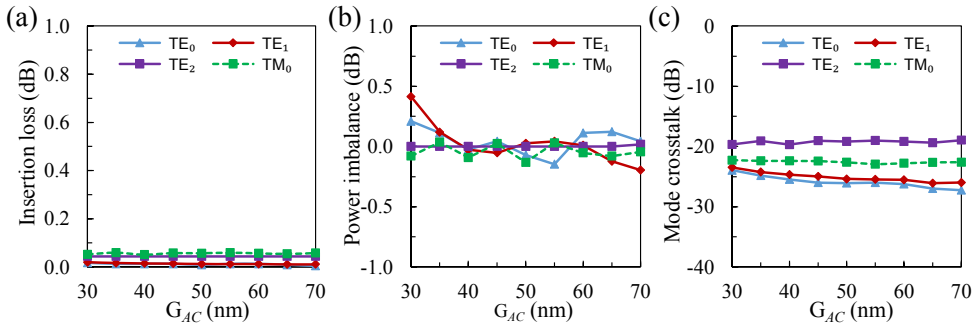

Fig. 10. Fabrication tolerance analysis to deviation of gap size (G_{AC}) at the output end of AC.

4. Conclusion

An ultra-broadband 3dB optical power splitter for multiple modes operation is proposed. An adiabatic coupler and an S-bend based Y-branch are adopted to split different modes simultaneously. To further validate this structure, we design a splitter for the four-lowest modes of a rib waveguides on SOI platform. By optimizing the geometrical parameters of the device, insertion losses less than 0.12 dB, power imbalances within ± 0.38 dB, and mode crosstalks below −18.5 dB are obtained for the four modes over a large wavelength band from 1400 nm to 1565 nm. In addition, the fabrication tolerance of gap size at the output end of adiabatic coupler is further investigated, showing a very stable device performance within a large deviation range of 40 nm. Although adiabatic process requires a long coupling length leading a large device footprint, the splitter has simple structure and is inherently broadband and tolerant to dimensional variations. The device concept could also be readily applied to other material systems, such as Si_3N_4 and Polymer.

Funding

Defense Advanced Research Projects Agency (DARPA).